The amplitude for $V \to V+j$ scalars is thus

$$A_{vv}{}^{ij} = \int du_1 \cdots du_{j-1}(2bK_1{}^i Q_1{}^j + yg^{ij}) I_u. \quad \text{(A7)}$$

A similar factorization of $V_s(q_1, \cdots, q_m)$ gives

$$A_{ss} = \int du_1 \cdots du_{j-1}(1-a-bM_1 Q_{10}) I_u. \quad \text{(A8)}$$

We then use another "charge-conjugation identity"

$$\int du_1 \cdots du_{j-1} K_{10} Q_{10} I_u = -\tfrac{1}{2} M_1 \int du_1 \cdots du_{j-1} Q_{10} I_u \quad \text{(A9)}$$

to write

$$\operatorname*{Res}_{\alpha(k_j{}^2)=1} \mathfrak{L} = A_{vv}{}^i + A_{ss} = \int du_1 \cdots du_{j-1} \times (1-a+2bK_i{}^\mu \cdot Q_{1\mu}+3y) I_u. \quad \text{(A10)}$$

This is to be compared to the pole in $\mathfrak{L}$ at $\alpha(k_j{}^2)=1$. The residue of that pole is the coefficient of $u_j{}^1$ in the integrand of (40). That we do, in fact, get (A10) may be checked using (4), (13), and (18).

In this calculation, we have explicitly factorized the poles into nonspurious particles. This sort of direct calculation is, in general, very complicated. Even to do the calculation up to first daughters for arbitrary J requires a messy diagonalization, and a general calculation seems impossible. Thus it is preferable to use the indirect approach of Secs. II and III.

PHYSICAL REVIEW VOLUME 185, NUMBER 5 25 SEPTEMBER 1969

High-Energy pp Scattering and Proton Substructure. IV

M. M. ISLAM
Physics Department, University of Connecticut, Storrs, Connecticut 06268

AND

JOE ROSEN*†
Physics Department, Brown University, Providence, Rhode Island 02912

(Received 8 May 1969)

Results of a systematic analysis of high-energy pp elastic-scattering data in terms of a proton-substructure model are presented. The model satisfactorily describes differential cross sections over the entire momentum range 5–31 GeV/c and over the whole angular interval 0°–90°. pp elastic differential cross sections at future accelerator energies (70, 200, and 1600 GeV) are also predicted. The model indicates that the proton has two hadronic core distributions, which interact via exchange of vector mesons ω (~800 MeV) and ω' (~2200 MeV). The rms radii of these distributions are 0.44 and 0.20 F.

I. INTRODUCTION

FROM optical-model considerations, it was pointed out some time ago[1] that the nucleon appears to consist of a number of hadronic distributions of increasing mean square radii and that the inner distributions, which are associated with heavier quanta, dominate the large-momentum-transfer scattering. Quantitative formulation of this model was done later by us,[2] taking into account absorptive corrections, and was applied to explain the 90° fixed-angle data of Akerlof *et al.*[3]

The model was further refined by incorporating Lorentz contraction of the hadronic distributions in the barycentric frame[4] and then used to analyze the pp elastic-scattering data of Allaby *et al.*[5] The vector-meson–nucleon form factors obtained from our pp scattering analysis were used to determine the proton magnetic form factor[6] and gave good agreement with the large-momentum-transfer data of Coward *et al.*[7] Recently, more data on pp scattering have been reported by the CERN group.[8] These data together

* Research supported by the U. S. Atomic Energy Commission Report No. NYO-2262TA-202.

† Present address: Physic, Department, Tel-Aviv University, Tel-Aviv, Israel.

[1] M. M. Islam, Nuovo Cimento **48**, 251 (1967); in *Lectures In Theoretical Physics*, edited by A. O. Barut and W. E. Brittin (Gordon and Breach, Science Publishers, Inc., New York, 1968), Vol. 10B, p. 97.

[2] M. M. Islam and Joe Rosen, Phys. Rev. Letters **19**, 178 (1967); **19**, 1360 (E) (1967), hereafter referred to as Paper I,

[3] C. W. Akerlof, R. H. Hieber, A. D. Krisch, K. W. Edwards. L. G. Ratner, and K. Ruddick, Phys. Rev. Letters **17**, 1105 (1966); Phys. Rev. **159**, 1138 (1967).

[4] M. M. Islam and Joe Rosen, Phys. Rev. **178**, 2135 (1969), hereafter referred to as Paper II.

[5] J. V. Allaby, G. Cocconi, A. N. Diddens, A. Klovning, G. Matthiae, E. J. Sacharidis, and A. M. Wetherell, Phys. Letters **25B**, 156 (1967).

[6] M. M. Islam and K. V. Vasavada, Phys. Rev. **178**, 2140 (1969).

[7] D. H. Coward *et al.*, Phys. Rev. Letters **20**, 292 (1968).

[8] J. V. Allaby *et al.*, Phys. Letters **27B**, 49 (1968); **28B**, 67 (1968).

with the small-angle data of the Brookhaven group[9] provide fairly complete pp angular distributions at a large number of energies. We therefore decided to investigate systematically whether our proposed model could describe this large amount of data and to this end carried out an extensive analysis of the pp elastic scattering. The purpose of this paper is to present the detailed results of the analysis, the conclusions we have been led to, and the pp differential cross sections predicted by our model at future accelerator energies. Some of the results of this investigation have already been briefly reported.[10]

A brief outline of the model is given in Sec. II. In Sec. III, an analytic approximation valid at large momentum transfer is discussed. Results of the analysis are presented in Sec. IV. Finally, in Sec. V a few concluding remarks are made.

II. OUTLINE OF THE MODEL

Briefly, the model is as follows. The elastic-scattering amplitude is represented in the impact-parameter form

$$f(s,\Delta)=ik\int_0^\infty bdb\,J_0(b\Delta)[1-e^{2i\delta(s,b)}], \tag{1}$$

where k is the c.m. momentum, $\Delta=2k\sin\frac{1}{2}\theta=(-t)^{1/2}$ is the momentum transfer, and s is the square of the c.m. energy. The differential scattering cross section is given by

$$d\sigma/dt=(\pi/k^2)|f(s,\Delta)|^2. \tag{2}$$

The phase-shift function $\delta(s,b)$ is assumed to consist of three parts[2];

$$\delta(s,b)=\delta_0(s,b)+\delta_1(s,b)+\delta_2(s,b). \tag{3}$$

$\delta_0(s,b)$ is completely determined by the diffraction scattering. Its detailed form is not explored; rather, its contribution is phenomenologically parametrized. $\delta_1(s,b)$ and $\delta_2(s,b)$ are treated in distorted-wave Born approximation (DWBA). The scattering amplitude in this approximation then becomes

$$f(s,\Delta)=ik\int_0^\infty bdb\,J_0(b\Delta)[1-e^{2i\delta_0(s,b)}] +2k\sum_{i=1}^{2}\int_0^\infty bdb\,J_0(b\Delta)e^{2i\delta_0(s,b)}\delta_i(s,b). \tag{4}$$

$\delta_1(s,b)$ and $\delta_2(s,b)$ are determined by two optical potentials with complex energy-dependent coupling constants. The radial dependence of these two potentials corresponds to the proton having two hadronic core distributions and interacting via exchange of heavy quanta. If the Lorentz contraction of these hadronic distributions is taken into account, then the Born amplitudes determining the optical potentials become[4]

$$f_{1,i}(s,\Delta)=-g_i(s)\frac{F_i^2(\tau^2)}{\Delta^2+\mu_i^2}. \tag{5}$$

Here,

$$F_i(\tau^2)=\{\beta_i(\tau^2+\mu_i^2)^{1/2}K_1[\beta_i(\tau^2+\mu_i^2)^{1/2}]\}^{1/2}$$

is the form factor corresponding to the Lorentz-contracted hadronic distribution

$$\tau=\Delta(1-\Delta^2/s)^{1/2}=k\sin\theta[1+4m^2\tan^2(\tfrac{1}{2}\theta)/s]^{1/2};$$

β_i determines the size of the distribution, and μ_i is the mass of the meson exchanged; $g_i(s)$ is the complex energy-dependent coupling constant. $\delta_1(s,b)$ and $\delta_2(s,b)$ can be directly obtained from (5) using the relation

$$\delta_i(s,b)=\frac{1}{2k}\int_0^\infty \Delta d\Delta\,J_0(b\Delta)f_{1,i}(s,\Delta). \tag{6}$$

The parametrization assumed by us for the diffraction part is

$$1-e^{2i\delta_0(s,b)}=(\sigma_T{}^d/\pi R^2)(1+i\epsilon)e^{-2b^2/R^2}. \tag{7}$$

$\sigma_T{}^d$ is the total diffraction scattering cross section; ϵ represents the real part of the diffraction amplitude; R determines the width of the diffraction peak. Inserting (6) and (7) in (4), we obtain

$$f(s,\Delta)=\frac{ik\sigma_T{}^d}{4\pi}(1+i\epsilon)e^{-R^2\Delta^2/8} +\sum_{i=1}^{2}\left\{f_{1,i}(s,\Delta)-\frac{\sigma_T{}^d}{4\pi}(1+i\epsilon)\int_0^\infty \Delta'd\Delta' \times f_{1,i}(s,\Delta')e^{-R^2(\Delta^2+\Delta'^2)/8}I_0(\tfrac{1}{4}R^2\Delta\Delta')\right\}. \tag{8}$$

To take into account the identity of the incident and the target protons, the triplet state should be antisymmetrized and the singlet state should be symmetrized. The differential cross section then takes the form

$$d\sigma/d\Omega=\tfrac{3}{4}|f(s,\Delta)-f(s,\Delta')|^2+\tfrac{1}{4}|f(s,\Delta)+f(s,\Delta')|^2, \tag{9}$$

where $\Delta'=2k\cos\frac{1}{2}\theta=(-u)^{1/2}$. Equation (8) provides the mathematical formulation of the present model. The next step is to use this amplitude to analyze the experimental data.

We see that the following parameters occur in the model. There are three parameters $\sigma_T{}^d$, R, and ϵ describing the diffraction scattering. It has been assumed throughout that these parameters are energy-independent.[11] There are four parameters describing each

[9] K. J. Foley *et al.*, Phys. Rev. Letters **11**, 425 (1963); **15**, 45 (1965).

[10] M. M. Islam and Joe Rosen, Phys. Rev. Letters **22**, 502 (1969), hereafter referred to as Paper III.

[11] In principle, some energy dependence should be included. However, from the point of view of our model, diffraction scattering is something unknown and phenomenologically described. Therefore, introducing too many parameters to describe it very accurately provides no further physical insight.

Born amplitude [Eq. (5)]: β_i, μ_i, $|g_i(s)|$, and arg $g_i(s)$. Of these, the first two are energy-independent, while the last two are energy-dependent.

III. ANALYTICAL APPROXIMATION FOR LARGE MOMENTUM TRANSFER

To get numbers from our model, the integral in Eq. (8) has to be numerically evaluated on a computer. This presents certain problems. One of them is that the function $f_{1,i}(s,\Delta')$ in the integrand becomes complex for $\Delta' > (s)^{1/2}$. However, because of the factor $e^{-R^2\Delta'^2/8}$, contribution to the integral from the region $\Delta' > (s)^{1/2}$ at high energy is negligible ($\frac{1}{8}R^2 s > 45$ for $p_L = 5$ GeV/c). The integral therefore can be cut off at $\Delta' = s^{1/2}$. Another problem, which is a serious one, occurs when Δ is large and therefore all the numbers involved are extremely small. Small errors in the numerical evaluation of the integral can then result in structures in the differential cross sections which are completely spurious. The problem becomes acute as the energy gets higher and we are able to go to very large momentum transfers. To overcome this difficulty, we have developed an analytic method for evaluating the integral in (8), which is reliable at large Δ. Let us now outline this method.

To simplify notation, we write $f_{1,i}(s,\Delta') = -g_i(s)\phi(\Delta'^2)$ [see Eq. (5)]. $\phi(\Delta'^2)$ depends on s also, but this is not explicitly exhibited. The integral in question is

$$I \equiv \int_0^\infty \Delta' d\Delta' \, \phi(\Delta'^2) e^{-R^2(\Delta^2+\Delta'^2)/8} I_0(\tfrac{1}{4}R^2\Delta\Delta'). \quad (10)$$

The crucial point to note is that for Δ large the main contribution to the integral comes from $\Delta' \approx \Delta$ region. This can be shown in the following way:

$$e^{-R^2(\Delta^2+\Delta'^2)/8} I_0(\tfrac{1}{4}R^2\Delta\Delta') \approx (2/\pi\Delta\Delta')^{1/2} R^{-1} e^{-R^2(\Delta-\Delta')^2/8}, \quad (11)$$

using the asymptotic form for the modified Bessel function $I_0(z)$. We can now write

$$I = \frac{4}{R^2}\int_0^\infty x^{1/2} dx \, \phi(\Delta^2 x^2) \frac{R\Delta}{2(2\pi)^{1/2}} e^{-R^2\Delta^2(1-x)^2/8} \quad (x = \Delta'/\Delta)$$

$$= \frac{4}{R^2}\int_0^\infty x^{1/2} dx \, \phi(\Delta^2 x^2)\delta(1-x), \quad (12)$$

if the limit $\Delta \to \infty$ is taken for the exponential and the following representation of the δ function is used:

$$\lim_{a\to\infty} (a/\pi^{1/2}) e^{-a^2x^2} = \delta(x).$$

We thus obtain for Δ large

$$I = (4/R^2)\phi(\Delta^2). \quad (13)$$

Once it has been established that the main contribution in evaluating I comes from the region $\Delta' \approx \Delta$ for Δ large, we can proceed in the following manner. Let us expand $\phi(\Delta'^2)$ in Eq. (10) around the value Δ^2:

$$\phi(\Delta'^2) = \phi(\Delta^2) + (\Delta'^2 - \Delta^2)\phi'(\Delta^2) + (1/2!)(\Delta'^2 - \Delta^2)^2\phi''(\Delta^2), \quad (14)$$

neglecting higher-order terms. Inserting (14) in (10), we get[12]

$$I = \tfrac{1}{2}\phi(\Delta^2)\int_0^\infty d(\Delta'^2) e^{-R^2(\Delta^2+\Delta'^2)/8} I_0(\tfrac{1}{4}R^2\Delta\Delta')$$

$$+\tfrac{1}{2}\phi'(\Delta^2)\int_0^\infty d(\Delta'^2)(\Delta'^2-\Delta^2) e^{-R^2(\Delta^2+\Delta'^2)/8} I_0(\tfrac{1}{4}R^2\Delta\Delta')$$

$$+\tfrac{1}{4}\phi''(\Delta^2)\int_0^\infty d(\Delta'^2)(\Delta'^2-\Delta^2)^2 e^{-R^2(\Delta^2+\Delta'^2)/8} I_0(\tfrac{1}{4}R^2\Delta\Delta')$$

$$= \frac{4}{R^2}\phi(\Delta^2) + \frac{1}{2}\left(\frac{8}{R^2}\right)^2\phi'(\Delta^2) + \frac{1}{2}\left(\frac{8}{R^2}\right)^2\left[\Delta^2 + \frac{8}{R^2}\right]\phi''(\Delta^2). \quad (15)$$

Since $\phi(\Delta^2)$ and its derivatives are known functions, (15) gives us an analytic expression for the integral. Higher-order corrections can easily be calculated by keeping more terms in (14). However, from numerical results we have found that keeping up to second derivative is sufficiently accurate. It should be noted that the right-hand side of (15) is actually energy-dependent, but the s dependence has been suppressed for clarity.

The advantage of (15) is that it can be evaluated directly and does not suffer from the uncertainties of numerical integration. In our analysis, angular distributions have been calculated using numerical integration routines and the formula (15). There is a region where both the numerical routines and approximation (15) give the same result. Beyond that, for larger Δ the integration routines become unreliable and often give spurious structures such as bumps. These bumps disappear if the integration accuracy is increased appreciably. Of course, it shows that the method is impractical. The dip-bump structures which occurred in Fig. 2 of Paper II, where all results were obtained using a numerical integration routine, are indeed spurious. The new results will be seen to be completely smooth.

IV. RESULTS OF ANALYSIS

As mentioned earlier, there are seven energy-independent and four energy-dependent parameters in our model. In principle, one expects that a least-squares curve-fitting method will determine the parameters reasonably well (we neglect errors of experimental points). In practice, we have found that this is not so.

[12] *Tables of Integral Transforms*, edited by A. Erdélyi (McGraw-Hill Book Co., New York, 1954), Vol. 1, p. 197.

While a curve-fitting method can yield rough values of the parameters, to get good fits we had to let the parameters vary over suitable ranges and then determine from the fits the best set of parameters. In this paper, the energy-independent parameters have been taken to be the same as in Paper II, but the energy-dependent parameters $g_1(s)$ and $g_2(s)$ have been left free. Note that in Paper II small-angle data were not used and not so much large-angle data were available at that time.

The fits obtained by us in the lab-momentum range 5–21 GeV/c and over the whole angular interval are shown in Figs. 1(a)–1(l), using conventional plots of $d\sigma/dt$ against $-t$. Values of the parameters are given in Tables I and II. Experimental points are taken from Allaby *et al.*,[5,8] Foley *et al.*,[9] Clyde,[13] Ankenbrandt *et al.*,[14] Harting *et al.*,[15] and Orear *et al.*[16] Satisfactory fits have been obtained throughout. Our fits in the diffraction region could be further improved by allowing some energy dependence of the diffraction parameters. However, we thought this was not warranted, since the model does not make any statement about the diffraction region except that it should be suitably parametrized. It should also be mentioned that a repulsive real part in the forward direction having the right magnitude is obtained by us.

To obtain angular distributions for lab momenta above 21 GeV/c, we have used the following parametrization for $|g_2(s)|$:

$$|g_2(s)| = A_2(s/m_p^2)^{\alpha_2}. \tag{16}$$

Arguments for such a parametrization have been given in Paper II. The values of A_2 and α_2 are 11.72×10^4 and -2.466, respectively. These values have been chosen to give reasonable fits [Figs. 1 (m) and 1 (n)] with the limited rough data available at 26 and 31 GeV/c.[17,18] arg $g_2(s)$ has been taken to be constant and has been given its value at 21 GeV/c. $|g_1(s)|$ and arg $g_1(s)$ have also been taken to have their values at 21 GeV/c. We have checked that if $|g_1(s)|$ is allowed an energy dependence like $|g_2(s)|$, the differential cross section is

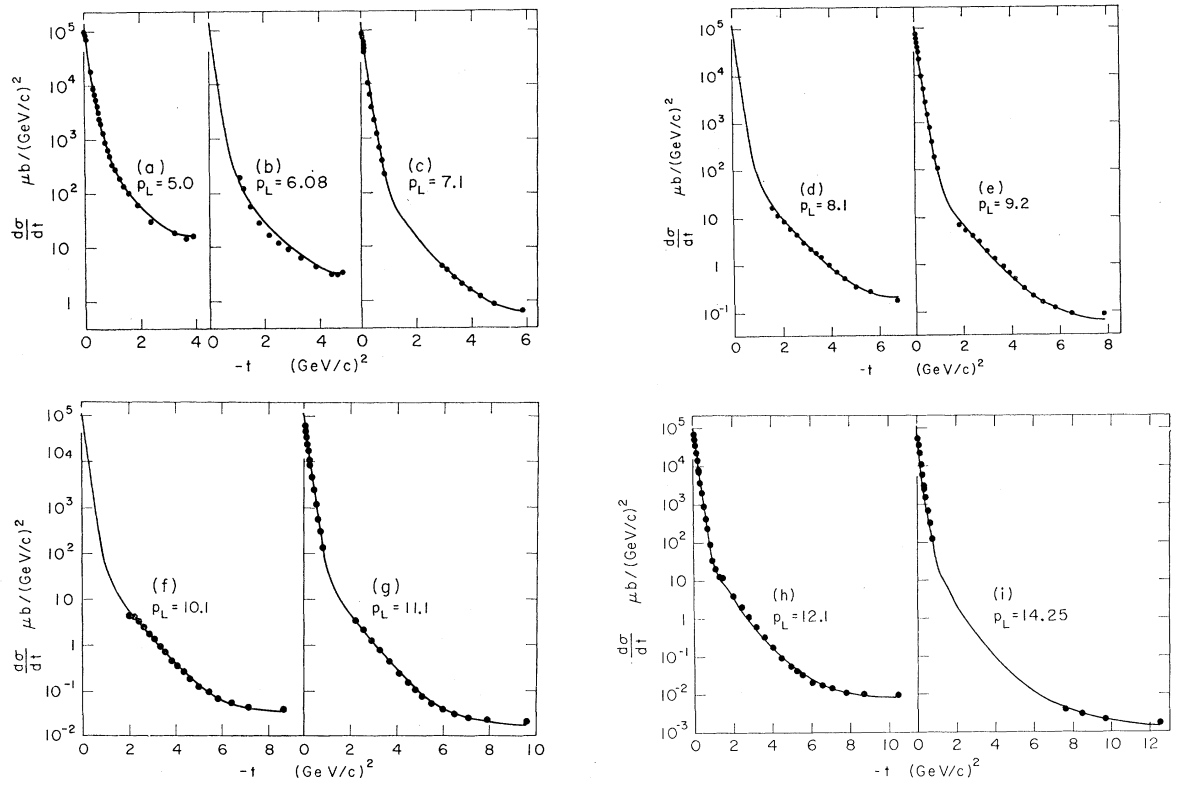

FIG. 1. (a)–(n) Solid curves represent fits to the experimental differential cross sections at various lab momenta. Experimental points (dark circles) are taken from Allaby *et al.* (Refs. 5 and 8), Clyde (Ref. 13), Ankenbrandt *et al.* (Ref. 14), Harting *et al.* (Ref. 15), Orear *et al.* (Ref. 16), Diddens *et al.* (Ref. 17), and Cocconi *et al.* (Ref. 18). (o)–(r) Predicted pp differential scattering cross sections at lab momenta 50, 70, 200, and 1600 GeV/c.

[13] A. R. Clyde, University of California Lawrence Radiation Laboratory Report No. UCRL-16275, 1966 (unpublished).
[14] C. M. Ankenbrandt *et al.*, Phys. Rev. **170**, 1223 (1968).
[15] D. Harting *et al.*, Nuovo Cimento **38**, 60 (1965).
[16] J. Orear *et al.*, Phys. Rev. **152**, 1162 (1966).
[17] A. N. Diddens *et al.*, Phys. Rev. Letters **9**, 108 (1962); **9**, 111 (1962).
[18] G. Cocconi *et al.*, Phys. Rev. **138**, B165 (1965).

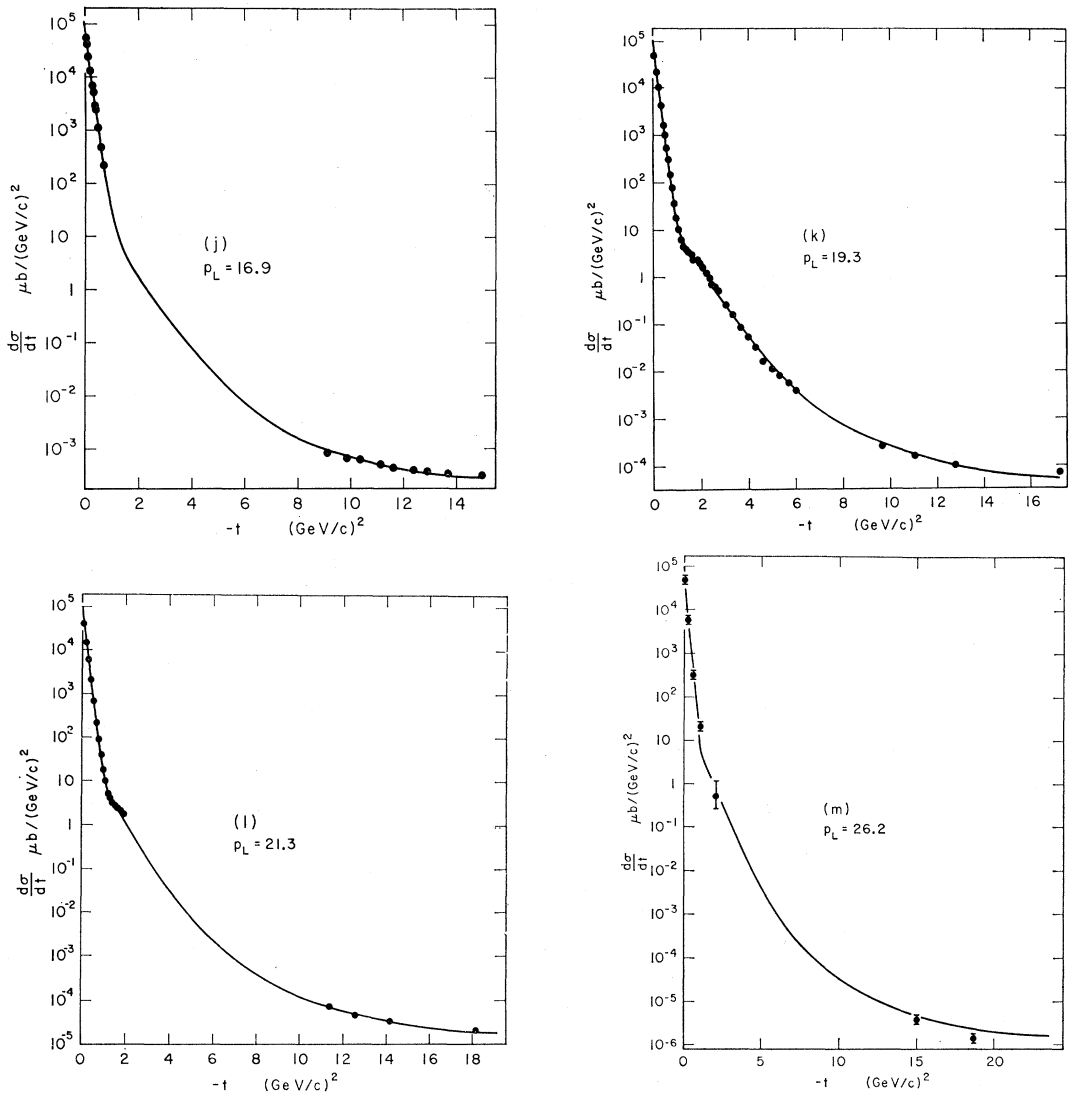

FIG. 1. (*Continued*).

not modified in any important way. It should also be pointed out that the angular distributions at high energies are insensitive to the phases of $g_1(s)$ and $g_2(s)$, since the effect of interference between the various amplitudes is small. Figures 1(o)–1 (r) are the predictions of our model at future accelerator energies (70 GeV/c, Serpukov; 200 GeV/c, Batavia; 1600 GeV/c, CERN colliding beam).

In Fig. 2, we have given the 90°-fixed-angle scattering predicted by our model from interpolation of the parameters $g_1(s)$ and $g_2(s)$, which have been determined

TABLE I. Values of the energy-independent parameters.

$\sigma_T{}^d$	R	ϵ	μ_1	μ_2	β_1	β_2
36.2 mb	1.2 F	0.249	0.801 GeV	2.163 GeV	0.615 F	0.338 F

TABLE II. Values of the energy-dependent parameters.

p_L (GeV/c)	5.0	6.08	7.1	8.1	9.2	10.1	11.1	12.1	14.25	16.9	19.3	21.3
$\lvert g_1(s)\rvert$ (GeV)	36.0	36.0	36.0	36.0	36.0	36.0	36.0	36.0	35.0	34.0	32.0	32.0
arg $g_1(s)$ (rad)	−0.248	−0.248	−0.248	−0.248	−0.248	−0.248	−0.248	−0.75	−0.90	−1.05	−1.25	−1.25
$\lvert g_2(s)\rvert$ (GeV)	151.0	103.0	63.98	52.97	42.25	39.50	36.97	33.00	22.00	16.00	10.30	8.75
arg $g_2(s)$ (rad)	−1.66	−1.66	−1.66	−2.26	−2.40	−2.68	−2.90	−3.6	−3.8	−3.75	−3.75	−4.15

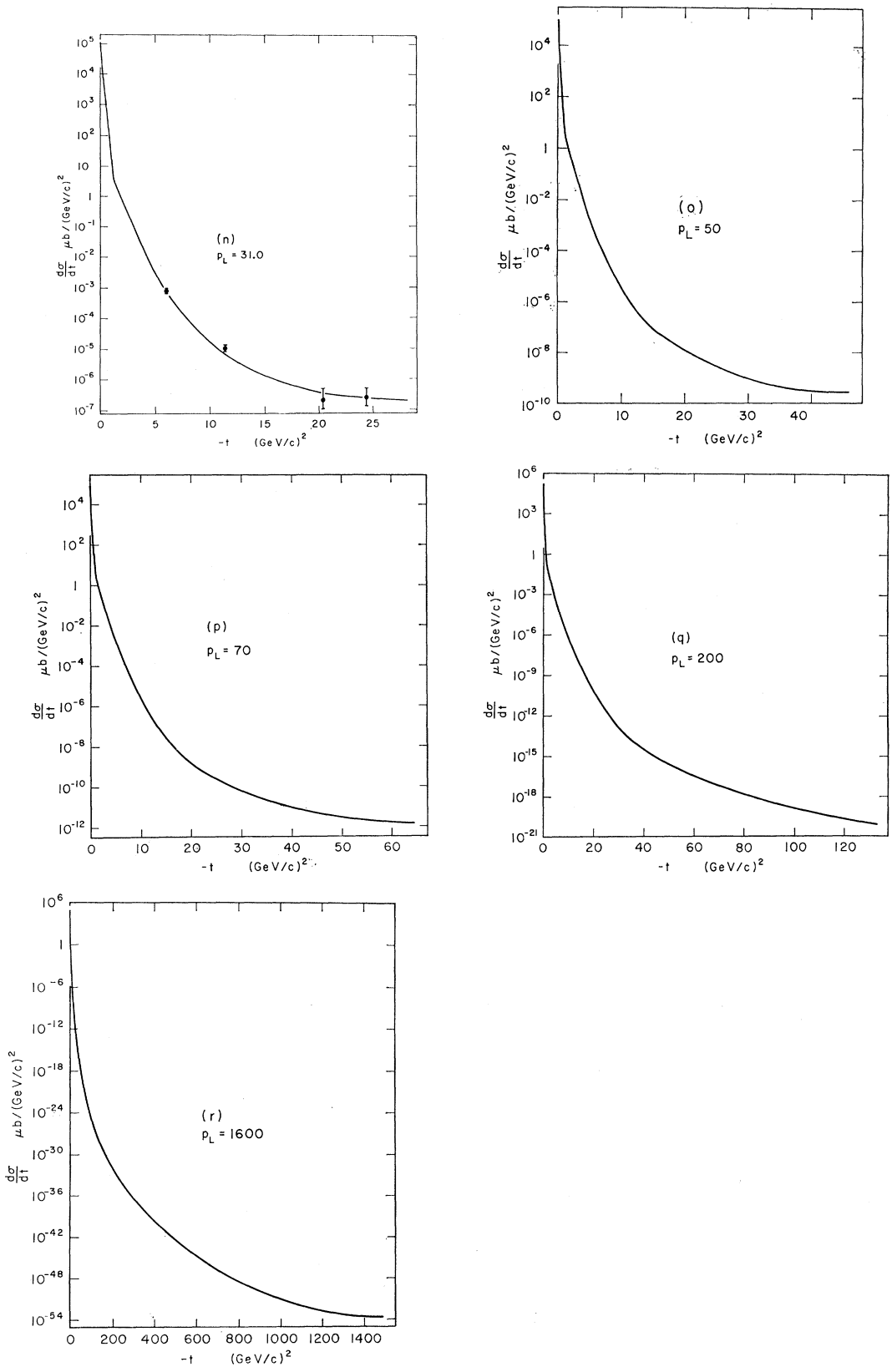

FIG. 1. (*Continued*).

from fixed energy data. The experimental points are those by Akerlof *et al.*[3] Since the theoretical curve is *not* a fit, but is obtained from interpolation, the agreement with experimental results is gratifying. In Fig. 3, we have shown the curve from which values of $|g_2(s)|$ have been interpolated. This is the only energy-dependent parameter which is important for 90° fixed-angle scattering. The dashed line is the extrapolation of $|g_2(s)|$, as given by the formula (16).

In Fig. 4, normalized differential cross sections $(d\sigma/dt)/(d\sigma/dt)_{t=0}$ are plotted against $-t$ for various lab momenta to indicate how pp elastic scattering changes as we go to higher and higher energies. The regularity with which pp angular distribution is varying is an important point to note.

In Fig. 5, $(d\sigma/dt)/(d\sigma/dt)_{t=0}$ is plotted for small $-t$. This figure shows that, in spite of our constant diffraction parameters, a shrinkage of the diffraction peak occurs. The shrinkage has already been noted in Paper II. The reason for it is that there is a large constructive interference term between the diffraction amplitude and the $i=1$ DWBA amplitude, and the interference term decreases with energy in the normalized differential cross section. Another point worth noting is that the shrinkage with energy is larger the further away we are from the forward direction. This explains why the CERN group did not see any shrinkage at small momentum transfers[19] $[-t\lesssim 0.1\ (\mathrm{GeV}/c)^2]$, while the Brookhaven group consistently observed shrinkage.[9]

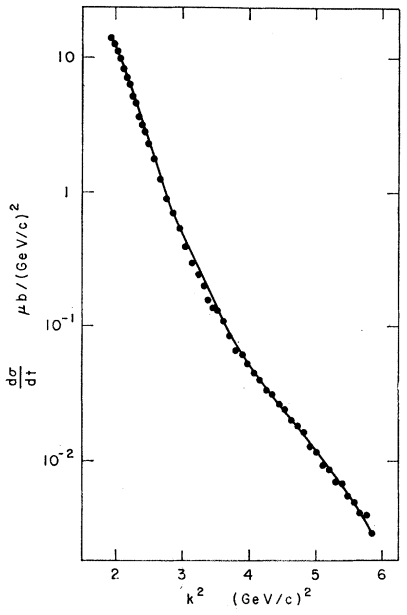

FIG. 2. Solid curve represents the 90° fixed-angle pp differential cross sections obtained from interpolation of the parameters $g_1(s)$ and $g_2(s)$. Experimental points are from Akerlof *et al.* (Ref. 3).

[19] G. Bellettini *et al.*, Phys. Letters **14**, 164 (1965); **19**, 705 (1966).

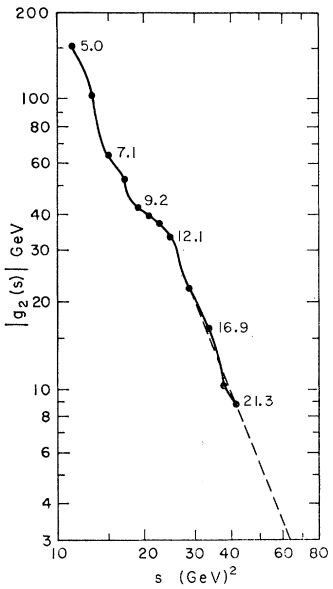

FIG. 3. Closed circles represent values of $|g_2(s)|$ determined from fixed-energy angular distributions. Solid line is a hand-drawn curve through these points. Values of $|g_2(s)|$ for the 90° fixed-angle scattering are interpolated from this curve. Dashed line is the extrapolation of $|g_2(s)|$ to higher energies according to the parametrization (16).

In Fig. 6, $d\sigma/d\Omega$ is plotted against the variable $\tau(\approx k_1)$ for both present accelerator energies as well as future accelerator energies. This type of data plot best exhibits the special features of the present model; namely, (i) the presence of a Gaussian diffraction peak at small values of τ, (ii) an Orear type of exponential

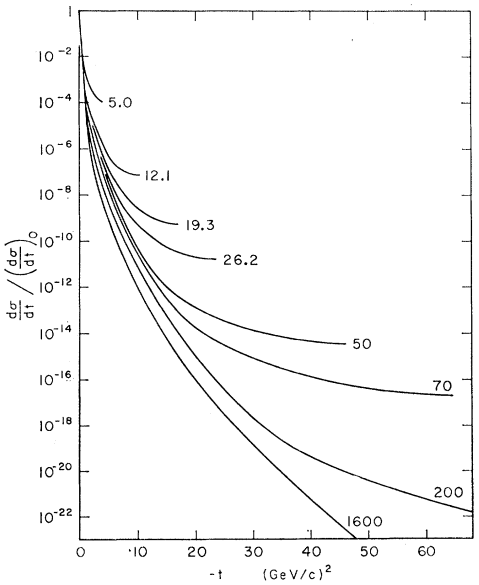

FIG. 4. Normalized pp differential scattering cross sections obtained in this paper at present and future accelerator energies. The curves show how the angular distribution varies with energy.

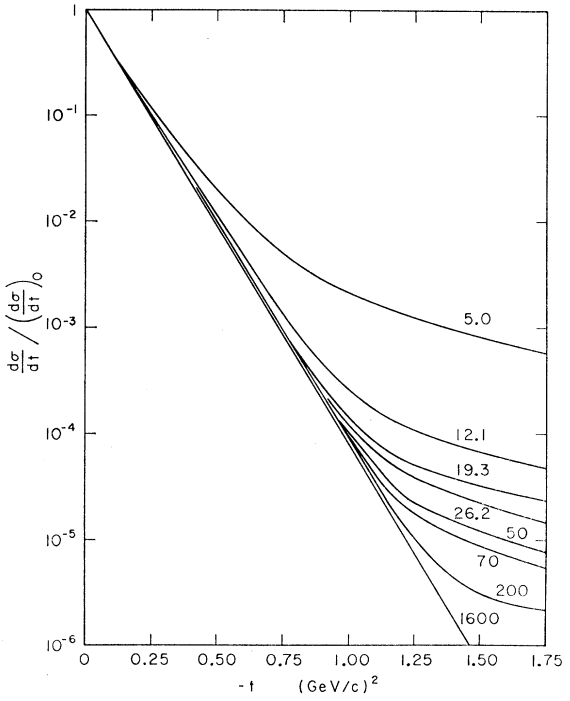

FIG. 5. $(d\sigma/dt)/(d\sigma/dt)_{t=0}$ plotted against $-t$ for small momentum transfers. The curves show energy variation of the diffraction peak obtained in this paper.

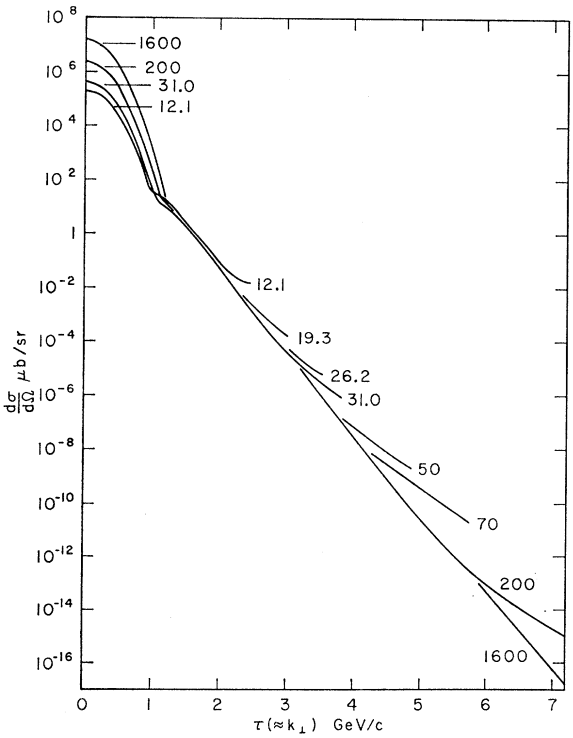

FIG. 6. Calculated differential scattering cross sections plotted against the variable τ ($\approx k_\perp$) for various values of the lab momenta.

fall[20] for intermediate values of τ, and (iii) a near-90° region with a flatter slope and strong energy dependence.

In Figs. 7(a)–7(c), we have shown similar plots for three different lab momenta 12.1, 26.2, and 70 GeV/c together with the individual contributions of the different amplitudes. These curves illustrate how the three amplitudes in Eq. (4) dominate three different regions in the angular distribution. Also, they show that the interference between the amplitudes becomes less important as the energy increases.

Finally, in Fig. 8, our normalized differential cross sections are compared with the fourth power of the proton magnetic form factor. The continuous curve is the form factor curve obtained by using the vector-meson–nucleon form factors predicted by the present model.[6] The short-dashed curve is the dipole fit. Large-momentum-transfer points are from Coward *et al.*[7] Our model predicts that the pp cross section is going to be appreciably below the proton form-factor curve when 70 GeV/c lab momentum is reached. This is in contrast to the model of Abarbanel, Drell, and Gilman,[21] who consider the form-factor curve to be the asymptotic limit of $(d\sigma/dt)/(d\sigma/dt)_{t=0}$.

V. CONCLUSION

The present paper completes a phenomenological investigation of high-energy pp elastic scattering which we started two years ago. We have found that the model proposed by us adequately describes all presently available pp elastic-scattering data both regarding their energy dependence and their angular dependence. In this model, large-angle scattering is associated with two hadronic core distributions of the proton and their Lorentz contraction. It has been argued[4] that these distributions interact via exchange of vector mesons ω and another one ω' having the same quantum numbers as ω. From the values of the parameters μ_i and β_i, the rms radii for these distributions can be calculated,[1] and they are 0.44 and 0.20 F. Further confirmation of the present model will strongly indicate that the proton has substructure.

From the point of view of our model, data plots which most stringently test its predictions are of the type in Fig. 6. In a plot of this nature, three regions characterized by their τ dependence and energy dependence should be seen at high s. The three regions correspond to the diffraction region, a region dominated by the $i=1$ amplitude, and a region dominated by the $i=2$ amplitude. This point has been discussed in detail in Paper III, so that we do not explore it any further. The discovery by the CERN group of two different slopes in a Orear-type plot[5] and the clustering of data points of different energies[8] for 1.2 GeV/$c \lesssim k_\perp \lesssim 2.0$

[20] J. Orear, Phys. Letters **13**, 190 (1964).
[21] H. D. I. Abarbanel, S. D. Drell, and F. J. Gilman, Phys. Rev. Letters **20**, 280 (1968); Phys. Rev. **177**, 2457 (1969).

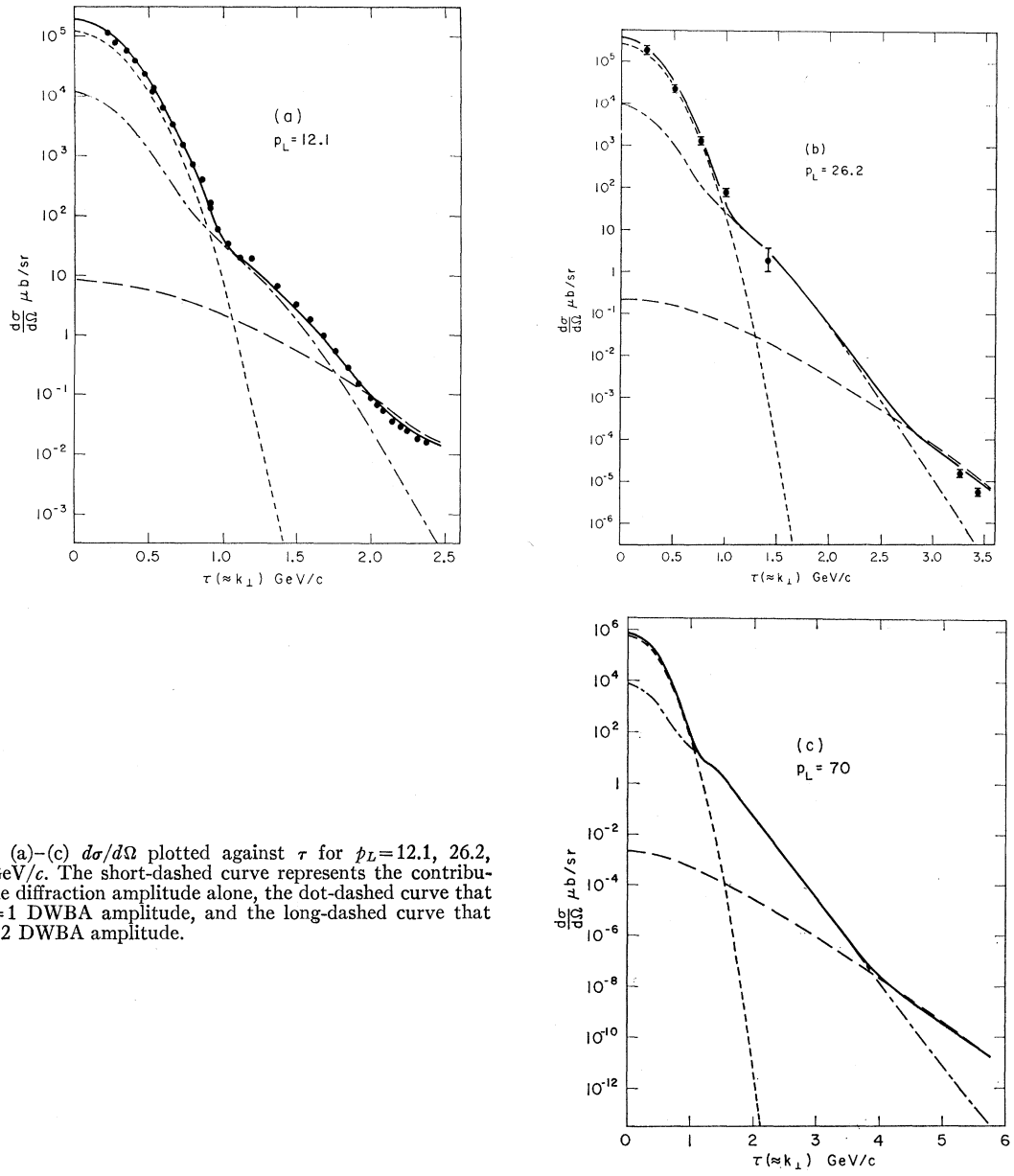

FIG. 7. (a)–(c) $d\sigma/d\Omega$ plotted against τ for p_L=12.1, 26.2, and 70 GeV/c. The short-dashed curve represents the contribution of the diffraction amplitude alone, the dot-dashed curve that of the i=1 DWBA amplitude, and the long-dashed curve that of the i=2 DWBA amplitude.

GeV/c are probably the best evidence in favor of our model.

One surprising result that has come out from this analysis is the following. Originally we started with this model[2] trying to explain the break phenomenon observed by Akerlof *et al.*[3] We attempted to explain the break as a transition from a region where the i=1 amplitude dominates to a region where the i=2 amplitude dominates. This would have meant that the phenomenon was indeed connected with the proton structure in our model. With the present analysis, which supercedes the earlier analysis, we find that the 2 i= amplitude completely dominates the 90° region and that this amplitude alone is sufficient to give a satisfactory agreement with the data of Akerlof *et al.* (see Fig. 2). Therefore, the break phenomenon is no longer connected with the transition from one region to another, rather with the energy dependence of the optical potential. We are thus led to conclude that while the existence of two Orear-type slopes in pp scattering is connected with the proton substructure, the break phenomenon of Akerlof *et al.* is connected with the inelastic production processes. Notice in Fig. 3 $|g_2(s)|$ changes in a very different way for 9.2 GeV/c

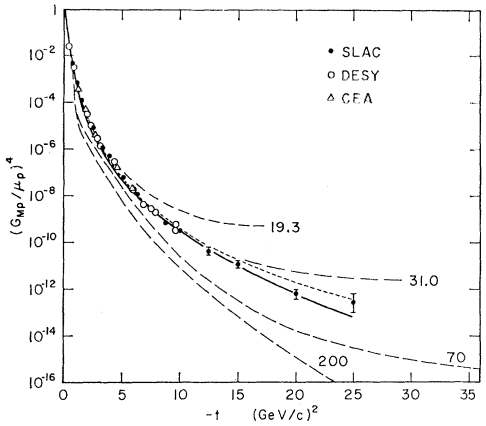

FIG. 8. Solid line is the theoretical form-factor curve obtained in Ref. 6. Short-dashed curve is the dipole fit. Long-dashed curves are the normalized pp angular distributions obtained in this paper at a number of lab momenta. Large-momentum-transfer data are from Coward *et al.* (Ref. 7).

$<p_L<12.1$ GeV/c. Other authors have also suggested a possible connection between the break phenomenon and the production processes.[5,22]

We would like to point out that various dip-bump structures obtained earlier in Fig. 2 of Paper II are spurious and were produced by the numerical integration routine. The analytic approximation which we have developed now [Eq. (15)] serves as an efficient check on any structure and provides an accurate evaluation of the integral at large momentum transfer.

Our plot of $(d\sigma/dt)/(d\sigma/dt)_{t=0}$ against $-t$ for various energies (Fig. 4) shows a systematic and smooth variation of pp elastic differential cross sections. This is in contrast to the Chou-Yang model, where dips should occur because of the diffraction zeroes.[23,24] In particular, the shoulder at $t\approx-1.5$ (GeV/c)^2 is interpreted in this model as evidence for the first dip structure and should accordingly become prominent with higher energy. In our model, it is associated with the transition to $i=1$ DWBA region and essentially remains the same even with considerable increase of energy [compare Fig. 7(a) with Figs. 7(b) and 7(c) at $\tau\approx1.0$ GeV/c]. This feature may experimentally distinguish between the Chou-Yang model and our model. Also, by 70 GeV/c we predict pp differential cross sections which fall below the asymptotic values predicted by the Chou-Yang model at $-t\gtrsim15$ (GeV/c)^2.

Finally, we mention some of the theoretical aspects of the present model. It has already been pointed out[25] that in this model the high-energy large-momentum-transfer scattering amplitude obeys the Mandelstam representation. Also, the vector-meson–nucleon form factors predicted by this model have the right analyticity and highly oscillatory spectral functions (see Appendix). For fixed t and $s\to\infty$, the model shows that only the diffraction scattering prevails: $d\sigma/dt=Ae^{R^2t/4}$. On the other hand, for θ fixed and $s\to\infty$, $d\sigma/d\Omega\sim e^{-2\beta_2 k_\perp}$ in conformity with results obtained from analyticity and boundedness.[26,27]

APPENDIX

It has already been shown in Ref. 25 that the form factor

$$F(t)=[\beta(\mu^2-t)^{1/2}K_1(\beta(\mu^2-t)^{1/2})]^{1/2} \tag{A1}$$

is analytic in the complex t plane except for a right-hand cut and vanishes for $|t|\to\infty$. The cut starts at $t=\mu^2$. Hence $F(t)$ obeys the following dispersion relation:

$$F(t)=\frac{1}{\pi}\int_{\mu^2}^{\infty}\frac{\mathrm{Im}F(t')dt'}{t'-t}. \tag{A2}$$

To determine the imaginary part of $F(t)$ on the cut, notice that for $t>\mu^2$ and $t=t+i0$,

$$\begin{aligned}&\beta(\mu^2-t)^{1/2}K_1(\beta(\mu^2-t)^{1/2})\\&=\tfrac{1}{2}\pi i\beta(t-\mu^2)^{1/2}H_1^{(1)}(\beta(t-\mu^2)^{1/2})\\&=\tfrac{1}{2}\pi i\beta(t-\mu^2)^{1/2}[J_1(\beta(t-\mu^2)^{1/2})\\&\qquad+iY_1(\beta(t-\mu^2)^{1/2})].\end{aligned} \tag{A3}$$

Therefore,

$$\begin{aligned}F(t)=&(\tfrac{1}{2}\pi\beta)^{1/2}(t-\mu^2)^{1/4}e^{i\pi/4}\\&\times[J_1^2(\beta(t-\mu^2)^{1/2})+Y_1^2(\beta(t-\mu^2)^{1/2})]^{1/4}\\&\times\exp\{\tfrac{1}{2}i\arctan[Y_1(\beta(t-\mu^2)^{1/2})/\\&\qquad J_1(\beta(t-\mu^2)^{1/2})]\}.\end{aligned} \tag{A4}$$

This gives

$$\begin{aligned}\mathrm{Im}F(t)=&(\tfrac{1}{2}\pi\beta)^{1/2}(t-\mu^2)^{1/4}\\&\times[J_1^2(\beta(t-\mu^2)^{1/2})+Y_1^2(\beta(t-\mu^2)^{1/2})]^{1/4}\\&\times\sin\{\tfrac{1}{4}\pi+\tfrac{1}{2}\arctan[Y_1(\beta(t-\mu^2)^{1/2})/\\&\qquad J_1(\beta(t-\mu^2)^{1/2})]\}.\end{aligned} \tag{A5}$$

For large t,

$$\mathrm{Im}F(t)=(\tfrac{1}{2}\pi\beta)^{1/4}(t-\mu^2)^{1/8}\sin[\tfrac{1}{2}\beta(t-\mu^2)^{1/2}-\tfrac{1}{8}\pi].$$

Hence the spectral function of the form factor oscillates very rapidly as $t\to\infty$. This is of course expected, since the discontinuity of a form factor, which falls off like $e^{-a|t|^{1/2}}$ as $t\to-\infty$ and is polynomially bounded, must oscillate infinitely many times.[28]

[22] J. J. J. Kokkedee and L. Van Hove, Phys. Letters **25B**, 228 (1967).
[23] T. T. Chou and C. N. Yang, Phys. Rev. Letters **20**, 1213 (1968).
[24] L. Durand, III, and R. Lipes, Phys. Rev. Letters **20**, 637 (1968).
[25] M. M. Islam, Phys. Rev. **178**, 2144 (1969).
[26] F. Cerulus and A. Martin, Phys. Letters **8**, 80 (1964).
[27] G. Tiktopoulos and S. B. Treiman, Phys. Rev. **167**, 1437 (1968).
[28] A. Martin, Nuovo Cimento **37**, 671 (1965).